# Morphologically Tunable Coassembly of Double Hydrophilic Block Polyelectrolyte with Oppositely Charged Fluorosurfactant

**ARTICLE** *in* MACROMOLECULES · OCTOBER 2014

Impact Factor: 5.8 · DOI: 10.1021/ma500622a



**4 AUTHORS:**

Mariusz Uchman
Charles University in Prague
**35** PUBLICATIONS **326** CITATIONS
SEE PROFILE

Stergios Pispas
National Hellenic Research Foundation
**303** PUBLICATIONS **5,527** CITATIONS
SEE PROFILE

Lubomir Kovacik
Charles University in Prague
**24** PUBLICATIONS **61** CITATIONS
SEE PROFILE

Miroslav Stepánek
Charles University in Prague
**56** PUBLICATIONS **712** CITATIONS
SEE PROFILE

Macromolecules

Article

pubs.acs.org/Macromolecules

# Morphologically Tunable Coassembly of Double Hydrophilic Block Polyelectrolyte with Oppositely Charged Fluorosurfactant

Mariusz Uchman,*[,†] Stergios Pispas,[‡] Lubomír Kováčik,[§] and Miroslav Štěpánek[†]

[†]Department of Physical and Macromolecular Chemistry, Faculty of Science, Charles University in Prague, Hlavova 2030, 128 40 Prague 2, Czech Republic

[‡]Theoretical & Physical Chemistry Institute, National Hellenic Research Foundation, 48 Vassileos Constantinou Avenue, 11635 Athens, Greece

[§]Institute of Cellular Biology and Pathology, First Faculty of Medicine, Charles University in Prague, Albertov 4, 128 01 Prague 2, Czech Republic

Supporting Information

**ABSTRACT:** We report on the formation and structure development of polyelectrolyte−surfactant complexes, PE−S, of double hydrophilic block copolymers poly(sodium 2-sulfamate-3-carboxylate isoprene)-*block*-poly(ethylene oxide), PSCI−PEO, and cationic fluorosurfactant, *N*-(3,3,4,4,5,5,6,6,7,7,8,8,9,9,10,10,10-heptadecafluorodecyl)-pyridinium chloride, HFDPCl. We compare the behavior of four PSCI−PEO samples differing in comonomer composition and polyisoprene block modification degree. Coassembled core−shell nanoparticles with the core formed by the PSCI/HFDPCl complex and the shell of PEO blocks were characterized by microscopic techniques (cryogenic transmission electron microscopy, atomic force microscopy) and by small-angle neutron scattering. Interactions between PSCI−PEO and HFDPCl were studied by isothermal titration calorimetry. We show that the bulky fluorosurfactant ions drive the coassembly toward structures with less curved interfaces such as cylindrical and wormlike micelles or vesicles. We also demonstrate the role of hydrophobic interactions in the system induced by the presence of unmodified polyisoprene units which in the case of the PSCI−PEO copolymer with a low degree of modification lead to formation of PSCI−PEO micelles and prevent the copolymer from the coassembly with HFDPCl.

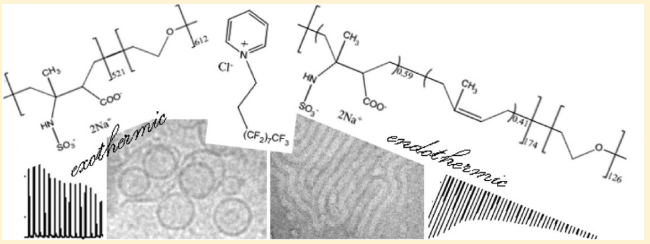


## INTRODUCTION

The double hydrophilic block polyelectrolytes (DHBE) and oppositely charged surfactants (S) coassemble into a variety of stimuli-responsive complex nanostructures (PE−S) like spherical micelles, vesicles, or wormlike micelles that differ in their detailed structural organization and offer applications in pharmaceutical, cosmetic, and food industry as detergents or vessels for solubilization and delivery of various hydrophobic substances.[1−6] To design PE−S coassembled nanostructures with required properties, a number of factors have to be taken into account, such as the polyelectrolyte and/or the chemical structure and surfactant concentration, molecular weight, charge density, backbone rigidity, and degree of branching of the polyelectrolyte as well as the polarity of the headgroup and the length of the aliphatic tail of the surfactant.[1−6]

Fluorosurfactants have proved to be promising contrast agents in $^{19}$F magnetic resonance imaging ($^{19}$F MRI), and their complexes with polymers allow for tailored preparation of nanoparticles formulations with high payloads.[7−12] Despite that, only a few studies on the formation of DHBEs and fluorosurfactants complexes have been performed so far,[11,12] and only little more is known about interaction of homopolymers and fluorosurfactants in solution.[13] In contrast, complexes of DHBE with hydrocarbon surfactants have been studied extensively.[1−6,14−21]

Interestingly, Laschewsky et al.[11] reported that the coassembly of perfluorodecanoic acid and DHBE containing cationic poly(trimethylammonium ethylacrytate) blocks lead to the formation of elliptical core−shell particles with the cores consisting of segregated lamellae of the fluorocarbon chains and polyelectrolyte the blocks. All the steps for the preparation of the above-mentioned nanoparticles were carried out in water and offer great potential for *in vivo* applications of such formulations. Such a strategy has a great advantage as compared to nanoparticles of amphiphilic block copolymers that are usually prepared using organic cosolvent and dialysis.

More recently, Wang and co-workers investigated association complexes of poly(ethylene glycol)-*b*-poly(sodium glutamate) ($PEG_{113}$−$PGlu_{50}$ and $PEG_{113}$−$PGlu_{100}$) and dodecyltrimethylammonium bromide surfactant (DTAB).[21] Differences in the association nanostructures, e.g., spherical and wormlike aggregates in $PEG_{113}$−$PGlu_{50}$/DTAB mixture and vesicular aggregates in $PEG_{113}$−$PGlu_{100}$/DTAB mixture, were explained

**Received:** March 26, 2014
**Revised:** September 4, 2014

   dx.doi.org/10.1021/ma500622a | *Macromolecules* XXXX, XXX, XXX−XXX

based on hydrophobic to hydrophilic balance and possible curvature of aggregates' interfaces. Fluorosurfactants themselves prefer to self-assemble into less curved interfaces as vesicles or elongated micelles due to their large excluded volume.[22]

This article is devoted to the formation and structure of PE-S nanoparticles composed of anionic−neutral DHBE, poly(sodium 2-sulfamate-3-carboxylate isoprene)-*block*-poly(ethylene oxide) copolymers, PSCI−PEO, and a cationic fluorosurfactant, *N*-(3,3,4,4,5,5,6,6,7,7,8,8,9,9,10,10,10-heptadecafluorodecyl) pyridinium chloride, HFDPCl, in alkaline aqueous solutions. We previously reported on the formation of wormlike micelles in the $PSCI_{174}$−$PEO_{126}$/HFDPCl system;[12] however, in this paper we show that the use of copolymers differing in both the degree of polymerization and the degree of polyisoprene block modification (see Table 1) allows for the formation of completely different PE−S nanostructures and, as we demonstrate, appreciably affects the process of the electrostatic coassembly and the properties of formed nanoparticles.

**Table 1. Molecular Characteristics of the Studied PSCI−PEO Block Copolymers and Their PI−PEO Block Copolymer Precursors**

| sample[a] | $M_{prec}$,[b] kg mol$^{-1}$ | $Đ_{prec}$[c] | $w(PI)_{prec}$[d] | $x(PI)_{PSCI}$[e] |
|---|---|---|---|---|
| $PSCI_{108}$−$PEO_{162}$ | 14.5 | 1.06 | 0.51 | 0.60 |
| $PSCI_{174}$−$PEO_{126}$ | 17.4 | 1.08 | 0.68 | 0.41 |
| $PSCI_{522}$−$PEO_{612}$ | 62.5 | 1.03 | 0.57 | 0.00 |
| $PSCI_{310}$−$PEO_{38}$ | 22.8 | 1.05 | 0.93 | 0.35 |

[a]Subscripts denote the degrees of polymerization of the corresponding blocks. [b]Weight-averaged molar mass of the PI−PEO precursor, determined by SEC in THF calibrated with PS standards. [c]Dispersity index of the PI−PEO precursor, determined by SEC. [d]Mass fraction of PI units in the precursor, determined by $^1$H NMR in $CDCl_3$. [e]Molar fraction of unmodified PI units in the PSCI block, determined by solid state $^{13}$C NMR.

The formation of PE−S complexes between PSCI−PEO and HFDPCl is studied by a combination of isothermal titration calorimetry (ITC), cryogenic transmission electron microscopy (Cryo-TEM), atomic force microscopy (AFM), and small-angle neutron scattering (SANS). The obtained data allow us to support the conclusions drawn from the previous article,[12] broaden the knowledge on the association of PE−S complexes containing fluorosurfactants, and demonstrate differences in the aggregation behavior as compared to the previously reported results.

## EXPERIMENTAL SECTION

**Materials.** The PSCI−PEO copolymers (Scheme 1a) were prepared by the postpolymerization reaction of polyisoprene-*block*-poly(ethylene oxide) (PI−PEO), prepared by living anionic polymerization,[23] with chlorosulfonyl isocyanate. Details on the synthesis can be found in ref 23. The weight-average molar masses of the PI−PEO precursors by SEC and the PSCI−PEO sample composition estimated by $^{13}$C solid state NMR are presented in Table 1. The PI block in the sample with high $M_w$ was fully modified; however, PI blocks in copolymers with lower $M_w$ were modified to some extent only as reveled by solid state $^{13}$C NMR (Scheme 1a). HFDPCl (Scheme 1b) was synthesized from 1*H*,1*H*,2*H*,2*H*-perfluorodecyl iodide and pyridine following the procedures outlined in ref 18.

PE−S complexes were prepared by mixing stock solutions of PSCI−PEO and HFDPCl. Stock solutions of PSCI−PEO and HFDPCl in 50 mM aqueous sodium tetraborate (pH 9.3) were mixed by stirring and left to stand for at least 24 h for equilibration prior to the measurements. The PSCI−PEO concentration in the solutions was 1 or 10 mg mL$^{-1}$.

**NMR Spectroscopy.** Solid state $^{13}$C NMR spectra were recorded on a Bruker Avance 500 spectrometer at 25 °C.

**Small-Angle Neutron Scattering (SANS).** SANS experiments were performed on the instrument D11 at the Institut Laue Langevin (ILL) in Grenoble, France. To cover a large *q*-range, measurements were done at a wavelength of 0.6 nm at sample-to-detector distances of 1.2, 8, and 32 m. Transmissions were measured with the attenuated direct beam at 8 m. Water was used as a standard to obtain absolute intensities and to account for the detector efficiency. $D_2O$ was used as a solvent to improve contrast and lower the incoherent background. Standard procedures[24] for data reduction were applied using the software package Bersans.[25]

**Isothermal Titration Calorimetry (ITC).** ITC measurements were performed at 25 °C with a Nano ITC isothermal titration calorimeter (TA Instruments - Waters LLC, New Castle, DE), equipped with a 24 karat gold reference and sample cells, both of 193 μL volume. The sample cell was connected to a 50 μL syringe, the needle of which was equipped with a flattened, twisted paddle at the tip, which ensured continuous mixing of the solutions in the cell rotating at 250 rpm. Titration was carried out by consecutive 1.03 μL injections of an aqueous 50, 25, 12.5, 6.25, and 3.12 mM HFDPCl in 50 mM sodium tetraborate solution from the syringe into the sample cell filled with an aqueous 1 g L$^{-1}$ PSCI−PEO block copolymer in 50 mM sodium tetraborate solution. A total of 48 consecutive injections were performed. The delay between two consecutive injections was 250−350 s. These injections replaced a part of the solution in the sample volume, and the changed concentration was considered in the calculation of the sample concentration. By this method, the differential heat of mixing was determined for discrete changes of composition. The data were analyzed using the NanoAnalyze software.

**Cryo-Transmission Electron Microscopy.** Cryo-TEM measurements were carried out using a Tecnai G2 Sphera 20 electron microscope (FEI Company, Hillsboro, OR) operated at the at the accelerating voltage of 120 kV, equipped with a Gatan 626 cryo specimen holder (Gatan, Pleasanton, CA) and a Gatan UltraScan 1000 slow scan CCD camera. The samples for Cryo-TEM were prepared by plunge-freezing as described earlier.[26] Briefly, 3 μL of the sample solution was applied to a glow-discharged (20 s at 5 mA current) electron microscopy grid covered with perforated carbon supporting film (C-flat 2/2-2C, Electron Microscopy Sciences). Most of the

**Scheme 1. Structures of (a) PSCI−PEO Copolymers[a] and (b) HFDPCl**

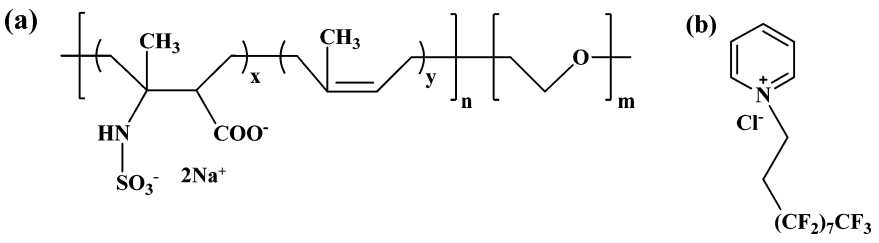


[a]$PSCI_{174}$−$PEO_{126}$: $x$ = 102, $y$ = 72; $PSCI_{108}$−$PEO_{162}$: $x$ = 43, $y$ = 65; $PSCI_{310}$−$PEO_{38}$: $x$ = 202, $y$ = 108; $PSCI_{521}$−$PEO_{612}$: $x$ = 512, $y$ = 0.


dx.doi.org/10.1021/ma500622a | *Macromolecules* XXXX, XXX, XXX−XXX

sample was removed by blotting (Whatman no. 1 filter paper) for approximately 1 s, and the grid was immediately plunged into liquid ethane held at −183 °C. The grid was then transferred into the microscope without rewarming. Images were recorded at microscope magnifications ranging from 3500× to 25 000× with a final pixel size ranging from 0.4 to 3 nm in the low dose image acquisition mode with the electron dose not exceeding 1500 electrons/nm$^2$. Typical values of the applied underfocus ranged between 0.5 and 2 $\mu$m. The applied blotting conditions resulted in an ice thickness varying between 100 and approximately 300 nm.

**Atomic Force Microscopy.** AFM measurements were performed in the tapping mode under ambient conditions using a commercial scanning probe microscope, Digital Instruments NanoScope dimensions 3, equipped with a Nanosensor silicon cantilever with a typical spring constant of 40 N m$^{-1}$. Polymeric micelles were deposited on a freshly peeled out mica surface, by a fast dip coating in a PSCI−PEO−HFDPCl aqueous solution ($c$ approximately $10^{-2}$ g L$^{-1}$). After evaporation of water, the sample was dried in a vacuum oven at ambient temperature for approximately 5 h.

## RESULTS AND DISCUSSION

The results of solid state $^{13}$C NMR spectroscopy (Figure 1) clearly indicate that about 60, 41, and 35% of isoprene units in

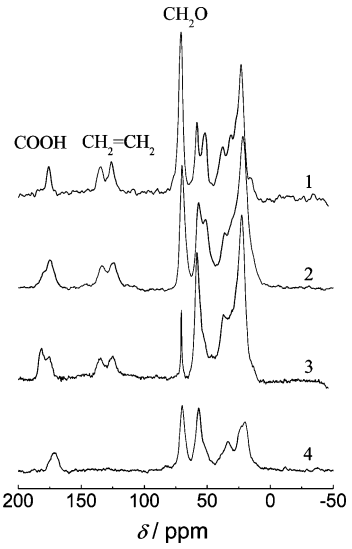


**Figure 1.** Solid state $^{13}$C NMR spectra of the (1) PSCI$_{108}$−PEO$_{162}$, (2) PSCI$_{174}$−PEO$_{126}$, (3) PSCI$_{310}$−PEO$_{38}$, and (4) PSCI$_{521}$−PEO$_{612}$ block copolymer.

the PSCI block of PISC$_{108}$−PEO$_{162}$, PISC$_{174}$−PEO$_{126}$, and PISC$_{310}$-PEO$_{38}$, respectively, have not been modified. Hence, the PSCI block should be regarded as a statistical copolymer (PSCI-*co*-PI) and has an amphiphilic rather than hydrophilic character due to the presence of hydrophobic nonfunctionalized isoprene units. In the case of PISC$_{521}$−PEO$_{612}$, all PI units have been modified successfully, as evidenced by the absence of peaks attributed to C=C bonds in the $^{13}$C NMR spectrum, resulting in a fully hydrophilic PSCI block.

**Micellization of HFDPCl in Sodium Tetraborate Buffer.** First, we studied the micellization of HFDPCl in 50 mM aqueous sodium tetraborate and in pure water in order to determine its cmc and to compare it with the values reported by other authors.[22] Figure 10a shows the typical measured raw heat changes as a function of time for the titration of 12.5 mM HFDPCl in 50 mM sodium tetraborate into the same buffer. Splitting of the micelles into individual surfactant molecules is accompanied by an endothermic effect. Above the cmc, when micelles are only being diluted, a less pronounced endothermic effect is observed. The data points in Figure 2 (black circles)

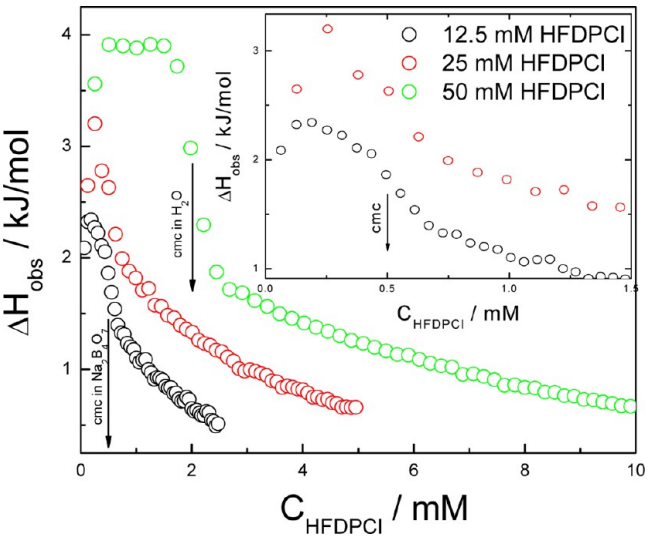


**Figure 2.** Enthalpy curves of titrating HFDPCl into $H_2O$ (green) and 50 mM sodium tetraborate buffer (red and black).

resulted from the integration of ITC peaks that appear in Figure 10a. The cmc was derived from the minimum of the first derivation of curves presented in Figure 2. Almgren et al.[22] determined the value of cmc of HFDPCl by surface tension measurements to be 2.6 mM in water and 0.4 mM in 50 mM NaCl. These values correspond very well to the results achieved by our ITC measurements, that is, 2.0 and 0.5 mM in water and in 50 mM sodium tetraborate, respectively.

The micellization process of ionic surfactants is much more complex as compared with nonionic surfactants. The repulsion between the head groups, the specific adsorption of counterions and the formation of an electrical double layer on surfactant micelles as well as the nature of the background electrolyte have a significant effect on the overall behavior of the studied system.[4,27−33] In order to determine the enthalpy of micellization properly, the initial concentration of the surfactant should be 20 times higher than the cmc.[27]

**Comicellization of HFDPCl Surfactant with PSCI−PEO Block Copolymers.** *Cryogenic Transmission Electron and Atomic Force Microscopy.* Cryo-TEM was used simultaneously with ITC experiments (discussed below) in order to characterize morphologies of PSCI−PEO/HFDPCl coassembled nanoparticles and to assign thermal effects observed by ITC to structural transitions in the PSCI−PEO/HFDPCl system. All Cryo-TEM samples were prepared from the solutions taken from the ITC experiments. When looking at the TEM micrographs of PSCI−PEO/HFDPCl particles, it is necessary to keep in mind that the compact core, containing electron-rich fluorine atoms intermixed with the PSCI block, has a much higher contrast than the solvated PEO shell which is almost invisible by Cryo-TEM. The copolymer concentration in all investigated solutions in 50 mM aqueous sodium tetraborate was 1 g L$^{-1}$, and the amount of added HFDPCl varied from 3.12 to 50 mM in order to cover the both regions with the excess negative charge of the SCI units ($COO^-$, $NHSO_3^-$) and the excess positive charge of HFDPCl. (The stoichiometric ratio between the surfactant and the polyelec-


dx.doi.org/10.1021/ma500622a | Macromolecules XXXX, XXX, XXX−XXX

trolyte units of PSCI, $Z$, is given by the molar concentrations of HFDPCl and SCI units as $Z$ = [HFDPCl]/[SCI].)

Figure 3 represents typical Cryo-TEM images of $PSCI_{174}$–$PEO_{126}$/HFDPCl nanoparticles obtained at $Z$ = 0.3 (A), 0.6 (B), and 1.2 (C). At $Z$ = 0.3, when the surfactant concentration reaches the cmc, the electrostatic interaction of the surfactant with charged PSCI block induces the formation of spherical micelles with the diameter ranging from 15 to 40 nm. As more surfactant is added, at $Z$ = 0.6, fairly polydisperse elongated structures are formed (Figure 3B). Those elongated structures grow from spherical micelles of $PSCI_{174}$–$PEO_{126}$/HFDPCl complexes interacting with each other (see inset in Figure 3B and Figure S1). The non-negligible amount of hydrophobic units of the functionalized PI block and the relatively short stabilizing PEO block promote anisotropic aggregation due to the large molar volume of the surfactant. A similar behavior was observed for the *in situ* prepared complexes of cadmium sulfide and PSCI–PEO block copolymer with the relatively short PEO block.[34] The elongated structures grow and accommodate more surfactant molecules with increasing $Z$. At $Z$ = 1, when the complex attains the zero net charge, compact core–shell elongated structures with the thickness of about 25 nm and the length up to several hundreds of nanometers appear in the solution (Figure 3C).

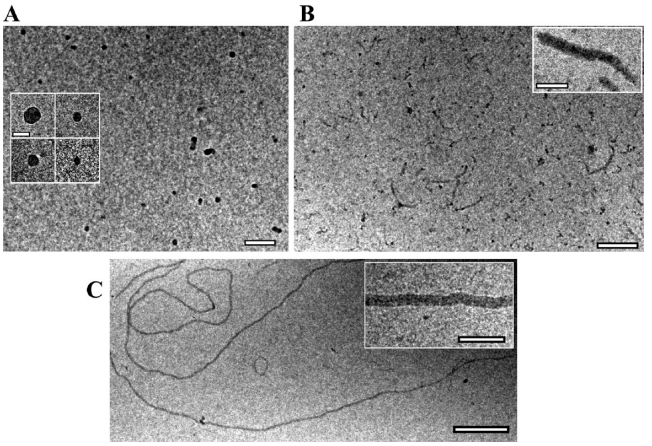


**Figure 3.** Cryo-TEM images of $PSCI_{174}$–$PEO_{126}$/HFDPCl complexes at different $Z$ ratios: (A) $Z$ = 0.3, scale bar 100 nm, inset 30 nm; (B) $Z$ = 0.6, scale bars 200 nm, inset 100 nm; and (C) $Z$ = 1.2, scale bars 500 nm, inset 100 nm.

The Cryo-TEM image of nanoparticles prepared at the high copolymer concentration (10 g $L^{-1}$) and $Z$ = 0.71 (Figure 4) reveals a large number of cylindrical micelles with the length of about hundreds of nanometers and the uniform thickness of 26 nm. Even though the shell is not visible due to the low contrast, the observed close packing of cylinders allows for the estimation of the PEO shell thickness, $l \sim 8$ nm.

When comparing the coassembly behavior of the $PSCI_{174}$–$PEO_{126}$/HFDPCl system with that of $PSCI_{108}$–$PEO_{162}$/HFDPCl which has roughly comparable lengths of the neutral hydrophilic and the polyelectrolyte blocks but differs significantly in the degree of modification of PI units (0.59 for $PSCI_{174}$–$PEO_{126}$ vs 0.40 for $PSCI_{108}$–$PEO_{162}$), we can see that the low solubility of the weakly modified and hydrophobic PSCI block in $PSCI_{108}$–$PEO_{162}$ leads to the formation of small spherical amphiphilic $PSCI_{108}$–$PEO_{162}$ micelles. The amount of the modified PI units is apparently too low to allow for the coassembly of $PSCI_{108}$–$PEO_{162}$ with HFDPCl surfactant into elongated core–shell nanoassemblies. Instead, at $Z$ = 0.3 small irregular nanoassemblies of $PSCI_{108}$–$PEO_{162}$/HFDPCl with 15 nm diameter (low contrast as compared with image in Figure 3A) are observed (Figure 5A). Further addition of HFDPCl

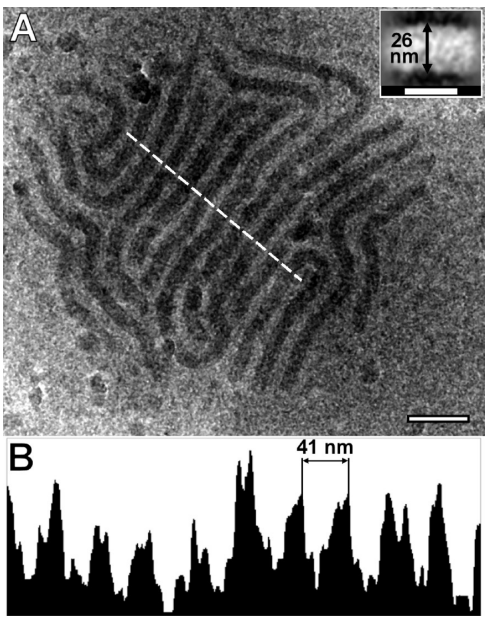


**Figure 4.** (A) Cryo-TEM image of $PSCI_{174}$–$PEO_{126}$/HFDPCl complex (copolymer concentration 10 g $L^{-1}$, $Z$ = 0.71). Scale bars: 100 nm inset 30 nm. Inset shows an average of straight short segments of the closely assembled micelles in reversed contrast. (B) Intensity profile through closely assembled micelles indicated in (A) by the white dashed line shows a period of about 41 nm. Since the average diameter of the cylindrical core of the particles measured as the full width at half-maximum (fwhm) is about 26 nm, the micelle-to-micelle spacing is then about 15 nm.

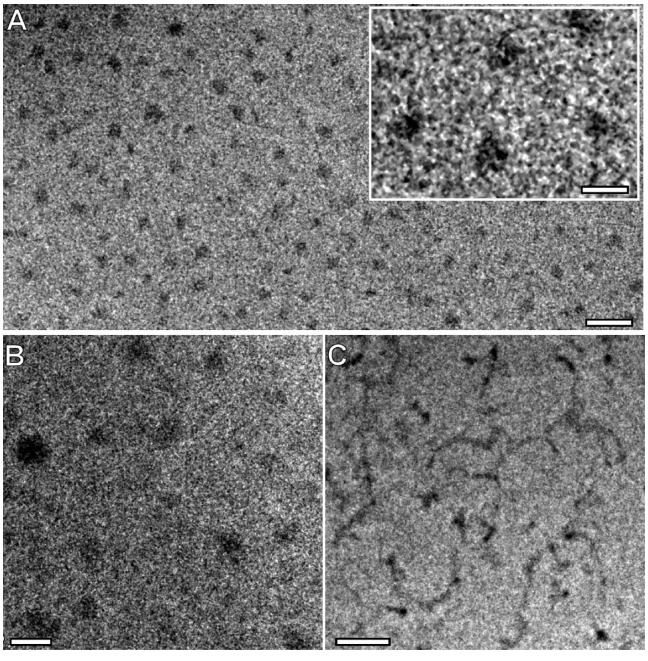


**Figure 5.** Cryo-TEM images of $PSCI_{108}$–$PEO_{162}$/HFDPCl complexes at different $Z$ molar ratios: (A) $Z$ = 0.3, scale bars 50 nm, inset 20 nm; (B) $Z$ = 1, scale bar 100 nm; and (C) $Z$ = 1, scale bar 50 nm.


dx.doi.org/10.1021/ma500622a | *Macromolecules* XXXX, XXX, XXX–XXX

surfactants, $Z$ = 1, promotes assembly of small micelles into bigger spherical aggregates (Figure 5B), but in addition individual threadlike micelles of HFDPCl can be observed (Figure 5C).

Figure 6 shows the nanoparticles formed by the $PSCI_{310}$–$PEO_{38}$/HFDPCl system at $Z$ = 0.8 and 1.8. In the case of

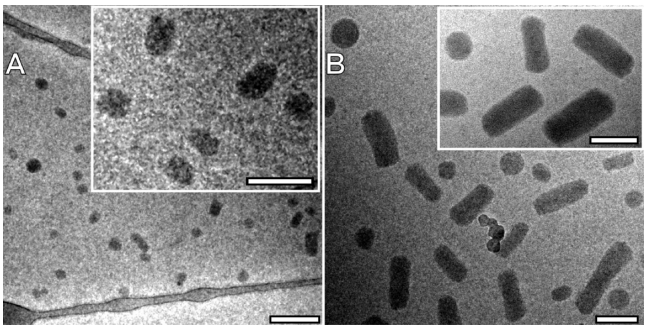


**Figure 6.** Cryo-TEM images of $PSCI_{310}$–$PEO_{38}$/HFDPCl complexes at different $Z$ molar ratios: (A) $Z$ = 0.8, scale bars 200 nm, inset 100 nm; (B) $Z$ = 1.8, scale bars 100 nm, inset 100 nm.

$PSCI_{310}$–$PEO_{38}$, the degree of PI block modification ($x$ = 0.65) is almost the same as in the case of $PSCI_{174}$–$PEO_{126}$ ($x$ = 0.59); however, the number of PSCI units is 2 times higher (202 vs 102, respectievly) and is sufficient for the coassembly of PSCI chains with the elongated surfactant micelles. Already at $Z$ = 0.8 oblate nanoparticles of about 50 nm diameter are observed. Interestingly, the thickness of short cylinders is twice higher than that of $PSCI_{174}$–$PEO_{126}$/HFDPCl nanoparticles (Figure 6B, $Z$ = 1.8). The PEO block is probably too short to stabilize the growth of wormlike micelles so that only short elongated particles can be observed on the Cryo-TEM micrographs.

It should be mentioned that the anisotropic assembly in the studied system is driven not only by HFDPCl, because especially the balance between the contribution of hydrophobic low glass transition temperature PI units and the PSCI units is an important parameter in anisotropic growth of core–shell nanoassemblies. It was shown that polybutadiene patches of multicompartment amphiphilic miktoarm star terpolymers micelles are responsible for the formation of hydrophobic bridges between micelles in water, resulting in formation of elongated nanostructures.[35]

In the case of the $PSCI_{521}$–$PEO_{612}$/HFDPCl complex at $Z$ = 0.27, Cryo-TEM revealed vesicular structures (the formation of which will be discussed in the ITC section) with thin walls of about 5 nm thickness (Figure 7 and Figure S2). The wall thickness is fairly monodisperse; however, the diameter of the vesicles has a broad distribution ranging from 40 to 160 nm.

We further employed AFM to investigate the behavior of PSCI–PEO/HFDPCl particles deposited on a freshly cleaved mica surface in the dry state. Figures 8A and 8B show 2 $\mu$m × 2 $\mu$m height scans (phase scans are shown as insets) of the $PSCI_{174}$–$PEO_{126}$/HFDPCl ($Z$ = 0.71) and $PSCI_{521}$–$PEO_{612}$/HFDPCl ($Z$ = 0.27) nanoparticles, respectively (for images of $PSCI_{310}$–$PEO_{38}$/HFDPCl and $PISC_{108}$–$PEO_{162}$/HFDPCl at $Z$ = 1.8 and 1, respectively, see Figure S3 in Supporting Information). Even though the nanoparticles are pancake-like deformed upon their deposition on the surface, their shapes are still well comparable with those measured *in situ* by Cryo-TEM. As expected, the height profiles of the nanoparticles significantly differ.

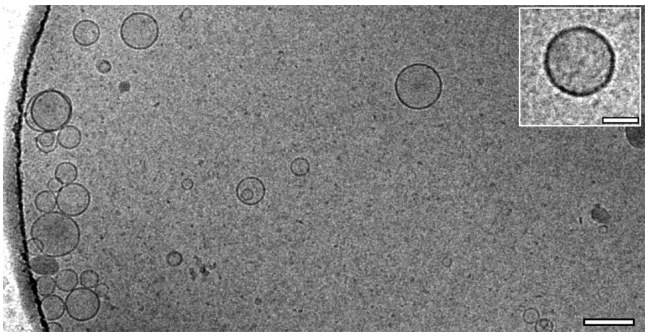

**Figure 7.** Cryo-TEM images of $PSCI_{521}$–$PEO_{612}$/HFDPCl at $Z$ = 0.27. Scale bar 200 nm, inset 50 nm.

Interestingly, the phase scans show that the nanoparticles consist of two distinct domains (hydrophilic hydrocarbon polymer and more hydrophobic fluorosurfactant) that differ significantly in viscoelastic properties. In the case of the $PSCI_{174}$–$PEO_{126}$/HFDPCl complex, the surfactant has tendency to agglomerate into small spherical objects embedded in the block copolymer matrix. However, in the case of $PSCI_{521}$–$PEO_{612}$/HFDPCl complexes, the surfactant seems to be well distributed all over the nanoparticles and does not seem to aggregate upon deposition and drying. Closer investigation of the large objects (inset in Figure 8b and Figure S4) allows for the observation of the stabilizing shell of the nanoparticles. It seems that the relatively short copolymer is more mobile on the surface than the copolymer with the high molecular mass. The latter allows for better stabilization of the complexes, that the surfactant molecules in the nanoparticles are unable to reorganize while drying on the mica surface.

*Small-Angle Neutron Scattering.* In order to confirm the formation of well-developed structures by $PSCI_{174}$–$PEO_{126}$/HFDPCl and $PSCI_{521}$–$PEO_{612}$/HFDPCl complexes (that is, wormlike particles and vesicles, respectively) revealed by Cryo-TEM, we employed SANS. Scattering curves of both PSCI–PEO/HFDPCl complexes are shown in Figure 9. The scattering curves exhibit oscillations characteristic for form factors of objects with spherical or cylindrical geometry. Since the oscillations are strongly suppressed by polydispersity of the scatterers and by instrumental smearing, the data allow only for a rough estimate of the minima positions which are shown in Figure 9. For the wormlike particles of the $PSCI_{174}$–$PEO_{126}$/HFDPCl complex (curve 1; the cylindrical structure is clearly indicated by the power law exponent −1 in the low $q$ region), the minima $q$ fulfill the condition $J_1(qR) = 0$, where $R$ is the cylinder radius and $J_1$ is the first-order Bessel function of the first kind. The first minimum, $q_1$, appears at ca. 0.21 $nm^{-1}$, which corresponds to the cylinder radius, $R_{cyl} = 3.83/q_1 = 18$ nm. For the vesicles formed by the $PSCI_{521}$–$PEO_{612}$/HFDPCl complex (curve 2) with the layer thickness much smaller than the radius of the vesicle, the form factor can be approximated by that of the thin spherical shell, $P(q) = [\sin(qR)/qR]^2$, where $R$ is the shell radius and the minima $q$ fulfill the condition $\sin(qR) = 0$. The first minimum, $q_1$, appears at ca. 0.07 $nm^{-1}$, which corresponds to the vesicle radius $R_{ves} = \pi/q_1 = 45$ nm. In both cases the dimensions obtained from the SANS curves correspond to the results of Cryo-TEM.

*Isothermal Titration Calorimetry.* In order to get information about thermodynamics, kinetics, and structural transitions of the coassembly process, the interaction of $PSCI_{174}$–$PEO_{126}$, $PSCI_{310}$–$PEO_{38}$, $PSCI_{108}$–$PEO_{162}$, and


dx.doi.org/10.1021/ma500622a | *Macromolecules* XXXX, XXX, XXX–XXX

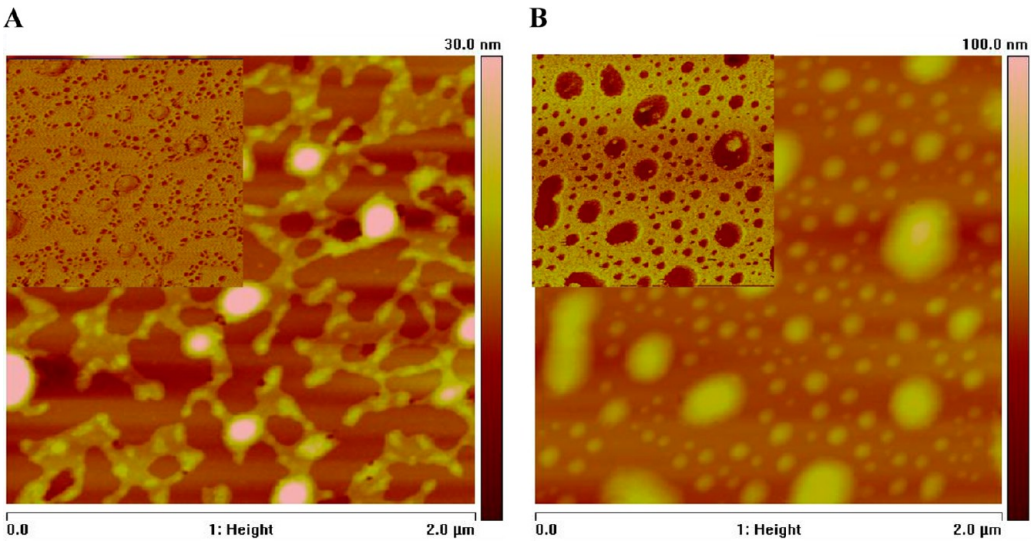


**Figure 8.** AFM images (top view) of the (A) $PSCI_{174}$–$PEO_{126}$/HFDPCl and (B) $PSCI_{521}$–$PEO_{612}$/HFDPCl nanoparticles at stoichiometric ratios $Z$ = 0.71 and 0.27. Phase scans are shown as insets.

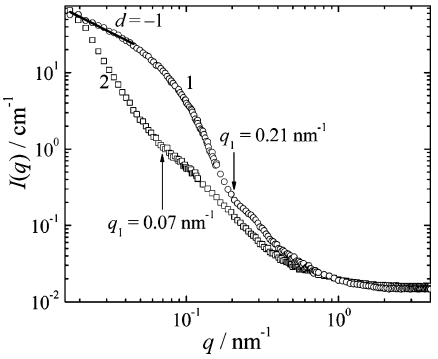


**Figure 9.** SANS curves for the $PSCI_{174}$–$PEO_{126}$/HFDPCl complex (curve 1; $Z$ = 0.71) and the $PSCI_{521}$–$PEO_{612}$/HFDPCl complex (curve 2; $Z$ = 0.27) in $D_2O$–buffer at 25 °C; the copolymer concentration is 2.5 mg mL$^{-1}$.

$PSCI_{521}$–$PEO_{612}$ with HFDPCl was monitored by ITC. The investigated interaction of PSCI–PEO with HFDPCl is a complicated process not only from the thermodynamic but also from the kinetic points of view, and thermal effects accompanying the appearance of individual structures are both exo- and endothermic (see Figure 10b–e). However, the demicellization and dilution of HFDPCl surfactant micelles is an endothermic process only (Figure 10a). In the case of $PSCI_{174}$–$PEO_{126}$ and HFDPCl, the exothermic contribution from electrostatic interactions smoothly decreases up to the eight addition (#8) of HFDPCl, that is, when reaching the cmc value of the pure surfactant, and then it is constant for the next few additions and then steeply decreases to the critical $Z \sim 0.45$ ratio. Further additions of HFDPCl resulted in an endothermic effect followed by a slow exothermic effect (see inset of Figure 10b). The isotherm in Figure 10b inset shows similarities with the data reported by Schillén et al. on a slow (>2000 s) well-defined sphere-to-worm transition upon interaction of poly(ethylene oxide)-*block*-poly(propylene oxide)-*block*-poly(ethylene oxide) triblock copolymer and hexa(ethylene glycol) monododecyl ether.[32] These similarities suggest that the fast endothermic process followed by a slower exothermic one could be attributed to the transition region between spherical micelles and wormlike nanoparticles (the sphere-to-worm transition) which is, however, much faster (~300 s) in our case.

The ITC raw data for $PSCI_{310}$–$PEO_{38}$/HFDPCl system (Figure 10d) followed almost the same pathway of thermal changes. Exothermic effects are not as pronounced as in the previous case; however, the endothermic ones are stronger, indicating additional cooperativity that could be explained by the higher content of PI units in PSCI block involving more hydrophobic interpolymer interactions in the nanoparticles formation. At ratio $Z$ = ~ 1.3, additional slow exothermic effects accompanied the fast endothermic one that was not visible in the previous case (inset in Figure 10d), indicating additional transformation or aggregation probably due to instability of nanoparticles (short PEO block).[36] For the $PSCI_{108}$–$PEO_{162}$/HFDPCl (Figure 10e) a strong exothermic effect lasts only to the seventh addition of HFDPCl and is followed by endothermic one. This transition is not that abrupt as in previous case. This difference can be explained on the basis of the Cryo-TEM results. HFDPCl interacts weakly with pre-formed micelles of $PSCI_{108}$–$PEO_{162}$, in which the PSCI blocks buried in the micellar core and are already strongly dehydrated so that the addition of HFDPCl causes no additional dehydration and endothermic enthalpy changes are not that pronounced.[33]

In the case of $PSCI_{521}$–$PEO_{612}$, the very first additions of HFDPCl are accompanied by strong exothermic effects which steeply grow to reach a maximum soon and immediately after they steeply decrease. At the $Z$ = ~0.2 ratio, that is, at significantly lower $Z$ ratio than in the case of $PSCI_{174}$–$PEO_{126}$/HFDPCl and $PSCI_{310}$–$PEO_{38}$/HFDPCl, an endothermic effect occurs, comparable with the effect accompanying the dilution of surfactant micelles in the buffer. This indicates that the binding of HFDPCl to the copolymer does not occur. However, just before that, the last exothermic peaks are followed by the second slow exothermic process lasting ~300 s, which indicates a transformation process (see #8 in Figure S5a). After a few more additions of HFDPCl, interestingly, the relatively fast endothermic process is followed by the second slow endothermic one (see Figure 10c and Figure S5b). This effect becomes pronounced by decreasing the isotherm baseline, which indicates the uptake (internalization) of


dx.doi.org/10.1021/ma500622a | *Macromolecules* XXXX, XXX, XXX–XXX

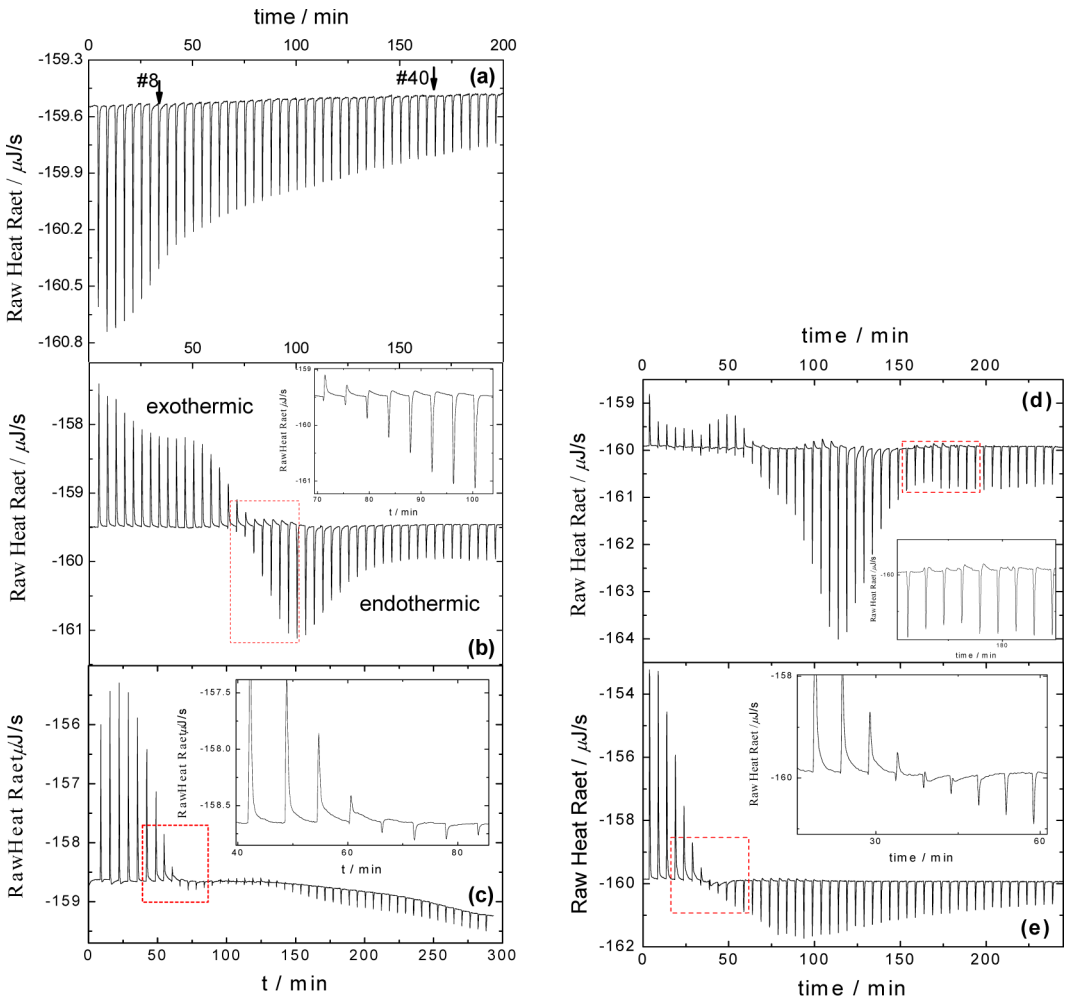


**Figure 10.** Thermograms showing the addition 50 $\mu$L of 12.5 mM HFDPCl into 193 $\mu$L of (a) 50 mM sodium tetraborate buffer, (b) 1 g $L^{-1}$ $PSCI_{174}$–$PEO_{126}$ (inset: magnification showing the fast endothermic process followed by a slower exothermic, sphere-to-worm transition), (c) 1 g $L^{-1}$ $PSCI_{521}$–$PEO_{612}$ (inset: magnification showing the slow exothermic process), (d) 1.1 g $L^{-1}$ $PSCI_{310}$–$PEO_{38}$ (inset: magnification showing the fast endothermic process followed by slower exothermic aggregation), and (e) 1.1 g $L^{-1}$ $PSCI_{108}$–$PEO_{162}$. Both HFDPCl and PSCI–PEO solutions were in 50 mM sodium tetraborate buffer.

HFDPCl molecules in the vesicles formed a few additions before. This kind of biphasic behavior was observed also by ITC for titration of vesicles of 1-palmitoyl-2-oleoyl-3-*sn*-glycerol-phosphatidylcholine, POPC, into the solution of surfactin.[37] Here the first fast endothermic reaction was attributed to the surfactin binding to the outer vesicles surface followed by a slower endothermic process of translocation of the molecule to the inner membrane and additional surfactin binding.

The curves in Figure 11 depict differential heats obtained by the integration of raw data during titration of 50 $\mu$L of 25 mM HFDPCl into different PSCI–PEO block copolymer buffered solutions (see also Supporting Information Figures S6 and S7).

Guo et al.[33] recently investigated the interaction between $\beta$-casein micelles and imidazolium-based ionic liquid surfactant by ITC. Spherical micelles of $\beta$-casein upon addition of imidazolium passed through different morphologies from large spherical aggregates to irregular complexes and interconnected network structure, redissociating finally into monodisperse spherical aggregates with a larger size. It is also noteworthy that the shape of the isothermal titration curves for the imidazolium surfactant into casein solution shows strong similarities to our results presented in Figure 11.

On the basis of the above-mentioned discussion and on the previously reported behavior of PE–S complexes of double hydrophilic block polyelectrolytes, we can summarize the ITC behavior of the PSCI–PEO/HFDPCl system in the following manner, distinguishing four regions ($C_0$, $C_I$, $C_{II}$, $C_{III}$, and $C_s$, Figure 11) with the corresponding critical $Z$ ratios:

(1) $PSCI_{174}$–$PEO_{126}$/HFDPCl and $PSCI_{310}$–$PEO_{38}$/HFDPCl (i) $C_I$, $Z < 0.2$: Exothermic noncooperative binding of the surfactant to the polyelectrolyte blocks at low $Z$ (see Figure S6a) (ii) $C_{II}$, $0.2 < Z < \sim 1$: In this region, first exothermic plateau is connected with additional cooperativity of HFDPCl binding and coassembly into spherical aggregates and their growth, the formation of which is promoted by the interaction of the surfactant with the partially hydrophobic (41 and 35% mol PI units, respectively) polyelectrolyte block. Further, the typical "cooperativity peak" is reflecting strong hydrophobic interaction between preformed micelles (reorganization of hydrophobic PI units and interaction of cooperatively bound surfactants); an isotropic growth occurs, resulting in the formation of long wormlike or cylindrical core–shell particles. (iii) $C_{III}$, $Z > \sim 1$: The growth process reaches a plateau ($PSCI_{174}$–$PEO_{126}$/HFDPCl) or minimum ($PSCI_{310}$–$PEO_{38}$/HFDPCl), indicating additional cooperativity due to favorable


dx.doi.org/10.1021/ma500622a | *Macromolecules* XXXX, XXX, XXX–XXX

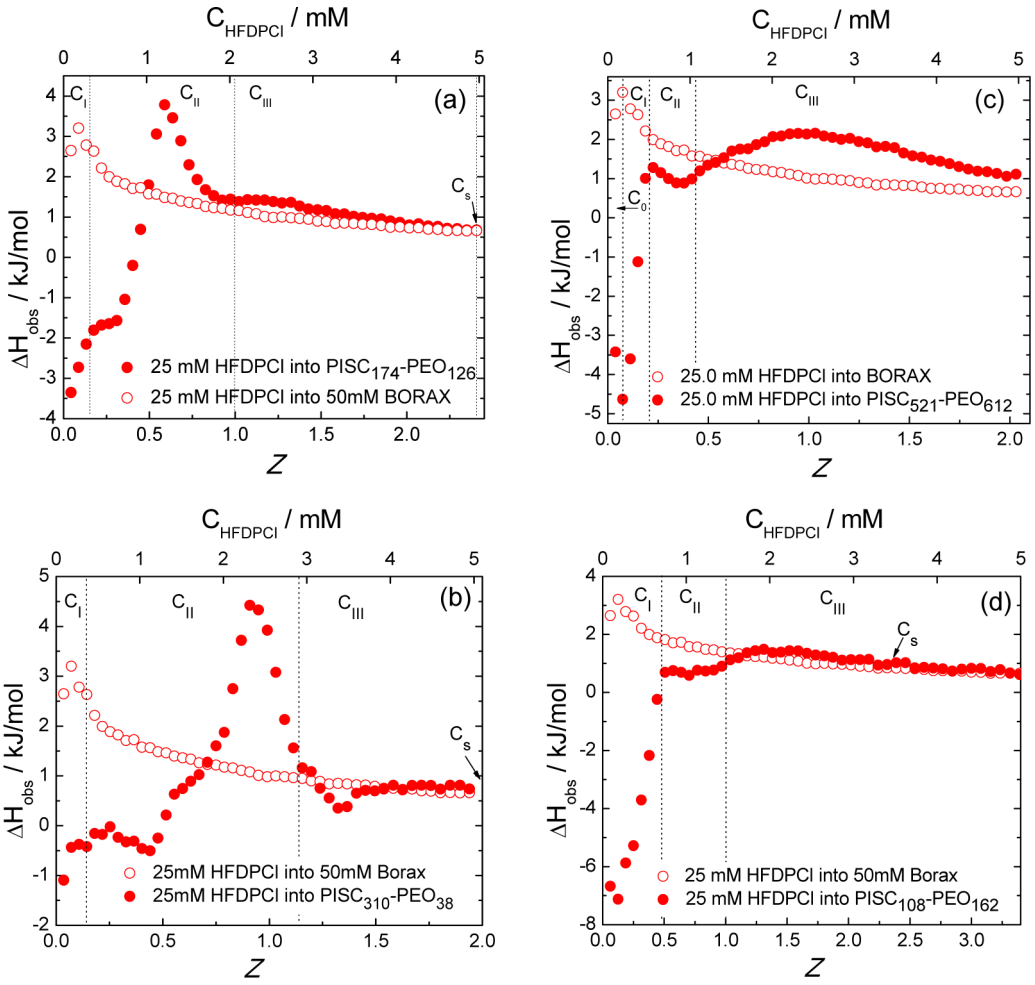


**Figure 11.** Enthalpy curves from titration of 25 mM HFDPCl into (a) 1 g $L^{-1}$ $PSCI_{174}$–$PEO_{126}$, (b) 1.1 g $L^{-1}$ $PSCI_{310}$–$PEO_{38}$, (c) 1 g $L^{-1}$ $PSCI_{521}$–$PEO_{612}$, and (d) 1.1 g $L^{-1}$ $PSCI_{108}$–$PEO_{162}$ in 50 mM sodium tetraborate solution (field circles) and into 50 mM sodium tetraborate buffer (open circles). The cmc value of HFDPCl at concentration of 0.5 mM.

hydrophobic interpolymer interaction.[38] (iv) $C_s$, $Z > \sim 2.8$: In this region, isotherms for the PSCI–PEO/HFDPCl system and for HFDPCl meet each other, indicating formation of free surfactant micelles in the solution.

(2) $PSCI_{521}$–$PEO_{612}$/HFDPCl and $PSCI_{108}$–$PEO_{162}$/HFDPCl. (i) $C_0$, $Z < 0.09$: The $PSCI_{521}$–$PEO_{612}$/HFDPCl enthalpy curve exhibit distinct minimum at $Z = \sim 0.09$. This behavior can be ascribed to the transition from noncooperative binding of the individual HFDPCl ions to cooperative binding of HFDPCl micelles[38] (more pronounced in titration with 12.5 mM HFDPCl; see Figure S7c). This behavior is markedly different to the previous and also missing in $PSCI_{108}$–$PEO_{162}$/HFDPCl systems. However, since both systems exhibit sterical hindrances for cooperative binding of bulky HFDPCl ions (in the case of $PSCI_{521}$–$PEO_{612}$ due to high charge density on the PSCI block and in the case of $PSCI_{108}$–$PEO_{162}$ due to limited space for the binding in the cores of $PSCI_{108}$–$PEO_{162}$ micelles, the noncooperative binding regime could be more pronounced in these two systems and last in region $C_I$. $C_{II}$, $Z > 0.25$ or 0.5: the structural transition of the PSCI–PEO/HFDPCl complex, segregation of the blocks and formation of the core–shell structures, which manifests itself as a distinct endothermic peak in both systems disused above. This behavior is very weakly developed for the $PSCI_{521}$–$PEO_{612}$/HFDPCl system (Figure 11c) and missing in the $PSCI_{108}$–$PEO_{162}$/HFDPCl system (Figure 11d). The enthalpy associated with the formation of thin-layer vesicles is very low in $PSCI_{521}$–$PEO_{612}$/HFDPCl system. The development of plateau at $Z > 0.5$ for $PSCI_{108}$–$PEO_{162}$/HFDPCl could be explained by the $PSCI_{108}$–$PEO_{162}$/HFDPCl micelles aggregation due to hydrophobic interaction and HFDPCl micelles formation as seen by Cryo-TEM. The ranges for both $C_{III}$ and $C_s$ regimes depend on the initial surfactant concentration as shown in the Supporting Information Figures S6 and S7. It has been shown that the way of mixing (surfactant into polymer or polymer into surfactant) is very important and leads to new information about equilibrium state of the complexes.[16,28] In order to conclude about the reversibility of the coassembly processes, we performed inverse ITC experiments which consisted in adding the copolymer solution into the HFDPCl solution. The thermograms from both experiments did not coincide which indicated that the coassembly is irreversible.

It is noteworthy that the behavior in the $C_{III}$ regime clearly differs from what was reported for many systems like poly(sodium acrylate)-*b*-poly(acrylamide) copolymer with dodecyltrimethylammonium bromide (DTAB),[28] poly(ethylene glycol)-*b*-poly(sodium glutamate) with DTAB,[21] or plasmid DNA with cobalt hexamine or spermidine,[39] where the formation of the core–shell structure was accompanied by a well-pronounced secondary endothermic peak which was


dx.doi.org/10.1021/ma500622a | *Macromolecules* XXXX, XXX, XXX–XXX

strongly dependent on the absolute concentration of the surfactant.

## CONCLUSIONS

Using a combination of microscopic (Cryo-TEM, AFM) techniques, SANS and ITC, we have demonstrated that the hierarchical coassembly of four different double hydrophilic block PSCI−PEO copolymers and the HFDPCl fluorosurfactant leads to a variety of nanostructures in aqueous solutions. By varying (i) the stoichiometric ratio between SCI units and HFDPCl, (ii) the copolymer and individual blocks length, and (iii) the hydrophilic modification degree of the polyisoprene block, the nanostructures formed can be tuned into a gamut of morphologies including spherical micelles with the core composed of the PSCI/HFDPCl complex and the PEO shell, short irregular worms (beads-on-string structures) and long core−shell cylinders ($PSCI_{174}$−$PEO_{126}$ copolymer) spherical aggregates incorporating low amounts of surfactant in coexistence with surfactant micelles ($PSCI_{108}$−$PEO_{163}$ copolymer), oblate nanoparticles or short cylinders ($PSCI_{310}$−$PEO_{38}$ copolymer), or vesicles ($PSCI_{521}$−$PEO_{612}$). The ITC measurements allowed us to investigate subtle thermal differences in the association behavior of the PSCI−PEO/HFDPCl systems and to precisely determine the stoichiometries corresponding to the formation of individual structures as well as shine light on the transformation kinetics of one nanostructure into another. In addition, ITC experiments demonstrated (i) the importance of hydrophobic interactions between unmodified monomeric units in the case of block copolymers with the lower degree of hydrophilic modification of the polyisoprene block, and the interrelationship between these interactions and the supramolecular structure formation in these particular systems of PE−surfactant complexes, and (ii) the irreversibility of the complexation process as well as its dependency on the mixing pathway, leading to the conclusion that these complex nanostructures should be considered metastable, but most probably kinetically frozen, at least for the time scale of the experiments.

Taking into account the biocompatibility of both components of the studied coassembly,[34,40] their chemical composition, and morphology characteristics, the prepared nanoparticles are prospective materials for nanomedicine (e.g., as probes in $^{19}F$ MRI or novel, structure tunable nanocarriers for pharmaceutical compounds).

## ASSOCIATED CONTENT

### Supporting Information

Figures S1−S7. This material is available free of charge via the Internet at http://pubs.acs.org.

## AUTHOR INFORMATION

### Corresponding Author

*E-mail mariuszuchman@go2.pl; Fax +420 22499752; Tel +420 221951292 (M.U.).

### Notes

The authors declare no competing financial interest.

## ACKNOWLEDGMENTS

The authors thank Dr. M. Urbanová from the Institute of Macromolecular Chemistry of the Academy of Sciences of the Czech Republic for samples characterization by $^{13}C$ solid state NMR and Dr. S. Prévost from TU Berlin, Germany for SANS measurements and discussion. The ILL (D11), Grenoble, France is acknowledged for beam time allocation. The authors acknowledge financial support from the Czech Science Foundation grants P208/12/P236 (M.U.) and P302/12/G157 (L.K.) and from the Charles University in Prague (grants Prvouk/1LF/1 and UNCE204022 to L.K.) and from the Ministry of Education, Youth and Sports of the Czech Republic (Grant 7AMB13PL026).

## REFERENCES

(1) Berret, J.-F. *Adv. Colloids Interface Sci.* **2011**, *167*, 38.
(2) Kogej, K. *Adv. Colloids Interface Sci.* **2010**, *158*, 68.
(3) Langevin, D. *Adv. Colloids Interface Sci.* **2009**, *147−148*, 170.
(4) Tam, K. C.; Wyn-Jones, E. *Chem. Soc. Rev.* **2006**, *35*, 693.
(5) Chiappisi, L.; Hoffmann, I.; Gradzielski, M. *Soft Matter* **2013**, *9*, 3896.
(6) Pispas, S. *Soft Matter* **2011**, *7*, 474.
(7) Ogawa, M.; Satoshi, N.; Aoki, H.; Ito, S.; Narazaki, M.; Matsuda, T. *Macromol. Chem. Phys.* **2010**, *211*, 1369.
(8) Knight, J. C.; Edwards, P. G.; Paisey, S. J. *RSC Adv.* **2011**, *1*, 1415.
(9) Peng, H.; Blakey, I.; Dargaville, B.; Rasoul, F.; Rose, S.; Whittaker, A. K. *Biomacromolecules* **2009**, *10*, 374.
(10) Ruiz-Cabello, J.; Barnett, B. P.; Bottomley, P. A.; Bulte, J. W. M. *NMR Biomed.* **2011**, *24*, 114.
(11) Laschewsky, A.; Mertoglu, M.; Kubowicz, S.; Thunemann, A. F. *Macromolecules* **2006**, *39*, 9337.
(12) Štěpánek, M.; Škvarla, J.; Uchman, M.; Procházka, K.; Angelov, B.; Kováčik, L.; Garamus, V. M.; Mantzaridis, Ch.; Pispas, S. *Soft Matter* **2012**, *8*, 9412.
(13) Hou, S.-S; Tzeng, J. K.; Chuang, M.-H. *Soft Matter* **2010**, *6*, 409.
(14) Hoffmann, I.; Heunemann, P.; Prévost, S.; Schweins, R.; Wagner, N. J.; Gradzielski, M. *Langmuir* **2011**, *27*, 4386.
(15) Uchman, M.; Štěpánek, M.; Prévost, S.; Angelov, B.; Bednár, J.; Appavou, M.-S.; Gradzielski, M.; Procházka, K. *Macromolecules* **2012**, *45*, 6471.
(16) Uchman, M.; Gradzielski, M.; Angelov, B.; Tošner, Z.; Oh, J.; Chang, T.; Štěpánek, M.; Procházka, K. *Macromolecules* **2013**, *46*, 2172.
(17) Jia, Z.; Truong, N. P.; Monteiro, M. J. *Polym. Chem.* **2013**, *4*, 233.
(18) Asakava, T.; Hisamatsu, H.; Miyagishi, S. *Langmuir* **1995**, *11*, 478.
(19) Nizri, G.; Magdassi, S.; Schmidt, J.; Cohen, Y.; Talmon, Y. *Langmuir* **2004**, *20*, 4380.
(20) Nizri, G.; Makarsky, A.; Magdassi, S.; Talmon, Y. *Langmuir* **2009**, *25*, 1980.
(21) Han, Y.; Xia, L.; Zhu, L.; Zhang, S.; Li, Z.; Wang, Y. *Langmuir* **2012**, *28*, 15135.
(22) Wang, K.; Karlsson, G.; Almgren, M.; Asakawa, T. *J. Phys. Chem. B* **1999**, *103*, 9237.
(23) Pispas, S. *J. Polym. Sci., Part A: Polym. Chem.* **2006**, *44*, 606.
(24) Chen, S. H.; Lin, T. L. In *Methods of Experimental Physics*; Price, D. L., Sköld, K., Eds.; Academic Press: New York, 1987; Vol. *23B*, p 489.
(25) Keiderling, U. *Appl. Phys. A: Mater. Sci. Process.* **2002**, *74*, S1455−S1457 ,Part 2 Suppl. S.
(26) Dubochet, J.; Adrian, M.; Chang, J. J.; Homo, J. C.; Lepault, J.; McDowall, A. W.; Schultz, P. Q. *Annu. Rev. Biophys. Biomol. Struct.* **1988**, *21*, 129.
(27) Olofsson, G.; Loh, W. *J. Braz. Chem. Soc.* **2009**, *20*, 577.
(28) Courtois, J.; Berret, J.-F. *Langmuir* **2010**, *26*, 11750.
(29) Rigsbee, D. R.; Dubin, P. L. *Langmuir* **1996**, *12*, 1928.
(30) Zheng, P.; An, X.; Peng, X.; Shen, W. *J. Phys. Chem. B* **2009**, *113*, 13566.
(31) Bai, G.; Wang, Y.; Yan, H.; Thomas, R. K.; Kwak, J. C. T. *J. Phys. Chem. B* **2002**, *106*, 2153.
(32) Löf, D.; Niemiec, A.; Schillén, K.; Loh, W.; Olofsson, G. *J. Phys. Chem. B* **2007**, *111*, 5911.

(33) Liu, Y.; Yang, L.; Guo, R. *Soft Matter* **2013**, *9*, 3671.
(34) Uchman, M.; Procházka, M.; Gatsouli, K.; Pispas, S.; Špírková, M. *Colloid Polym. Sci.* **2011**, *289*, 1045.
(35) Walther, A.; Müller, A. H. E. *Chem. Commun.* **2009**, 1127.
(36) Matejicek, P.; Brus, J.; Jigounov, A.; Plestil, J.; Uchman, M.; Prochazka, K.; Gradzielski, M. *Macromolecules* **2011**, *44*, 3847.
(37) Heerklotz, H.; Seelig, J. *Biophys. J.* **2001**, *81*, 1547.
(38) Lapitsky, Y.; Parikh, M.; Kaler, E. W. *J. Phys. Chem. B* **2007**, *111*, 8379.
(39) Matulis, D.; Rouzina, I.; Bloomfield, V. A. *J. Mol. Biol.* **2000**, *296*, 1053.
(40) Uchman, M.; Štěpánek, M.; Prochazka, K.; Mountrichas, G.; Pispas, S.; Voets, I. K.; Walther, A. *Macromolecules* **2009**, *42*, 5605.